A Two-Grid Overset Method for the Prediction of Isolated Rotor Hover Performance

Marvin A. Moulton[1], Mahendra J. Bhagwat[2], and Francis X. Caradonna[3]

[1]US Army AMRDEC, Aviation Engineering Directorate, Restone Arsenal, AL, USA
(Tel: +1-256-313-9024, E-mail: marvin.moulton@us.army.mil)

[2]US Army AMRDEC, Aeroflightdynamics Directorate, Ames Research Center, Moffett Field, CA, USA
(Tel: +1-650-604-2893, E-mail: bhagwat@merlin.arc.nasa.gov)

[3]US Army AMRDEC, Aeroflightdynamics Directorate, Ames Research Center, Moffett Field, CA, USA
(Tel: +1-650-604-5902, E-mail: caradonna@merlin.arc.nasa.gov)

Abstract: This paper concerns the development of an overset/hybrid method with a free-wake capability. The method utilizes three grid topologies: an H-grid to accurately convect the shed rotor wake utilizing Vorticity Embedding; an intermediate, full-potential C-grid to permit smooth coupling of the different flow solvers; and a near-blade C-grid to resolve the viscous flow including separation effects. Since the Eulerian near-blade solver is not burdened with resolving the shed vorticity, the method is grid point efficient. Previous applications of this technology have concentrated upon the near-blade viscous solution. However, this paper describes a new level of fidelity for the overset/hybrid method whereby the intermediate, full-potential C-grid extends to the blade surface to resolve the loads. This new two-grid overset option is exercised by predicting the isolated hover performance of the Knight and Hefner rotor which provides a first evaluation of this free-wake method.

Keywords: hover performance, full-potential, Vorticity Embedding, CFD

NOMENCLATURE

AR = blade aspect ratio, R/c
C_p = coefficient of pressure
C_Q = gross torque coefficient
C_T = gross thrust coefficient
C_q = sectional thrust coefficient, $C_d c(r)(r/R)^3$
$c(r)$ = local chord length
c = reference chord length
$\hat{E}, \hat{F}, \hat{G}$ = inviscid flux vectors
e = total energy per unit volume
J = Jacobian of transformation
$\mathcal{H}$ = matrix of primitive metrics
M_T = hover tip Mach number
$\hat{Q}$ = vector of conserved quantities
$\vec{q}$ = velocity vector
R = rotor tip radius
Re = Reynolds number
$\hat{\mathcal{R}}$ = source term accounting for blade motion
r = radial location
$\vec{r}$ = position vector
$\hat{S}$ = viscous flux vector
U, V, W = contravariant velocity components in the $\xi-$,$\eta-$ and $\zeta-$ directions, respectively
u, v, w = velocity components in the $x-$,$y-$ and $z-$ directions, respectively
x, y, z = Cartesian coordinates
Γ = bound circulation
γ = ratio of specific heats for a perfect gas
λ = shape function used in wake modeling
ξ, η, ζ = generalized computational coordinates
π = mathematical constant $(3.14159265...)$
ρ = density
τ = time in computational domain
$\theta_{.75}$ = collective pitch
Φ = velocity potential
Ω = angular velocity of rotating blade
Ψ = wake azimuth angle

Superscripts

T = transpose of matrix
v = vortical component

Subscripts

c = root chord length
i = induced effects
t = real time
x, y, z = pertaining to Cartesian coordinates
ξ, η, ζ = pertaining to generalized coordinates
τ = time in computational domain

Computer Codes

HELIX-I = original three-dimensional full-potential

solver equipped with Vorticity Embedding to compute rotor-wake interactions(H-H topology)

HELIX-IA = enhanced version of HELIX-I

HELIXC = two-grid overset version of HELIX-I (C-H and H-H topologies)

PLOT3D = graphics program designed to visualize grids and solutions of CFD

TURNS = three-dimensional Euler/Navier-Stokes solver for computing rotor-wake interactions(C-H topology)

1. INTRODUCTION

The flow fields about helicopter rotors are among the most challenging in aerodynamics, because of the diversity of flow phenomena that must be accurately modeled in order to predict the blade loading and performance. These phenomena include: compressibility effects, a complex vortex structure, and viscous effects. In particular, the the prediction of helicopter rotor wakes is one of the most enduring problems for Computational Fluid Dynamics (CFD) methods. The essential problem associated with most CFD methods is numerical in nature. That is, the numerical dissipation of currently known Eulerian methods is so rapid that it does not permit accurate modeling of global rotor problems that include both the rotor and its wake system.

This paper concentrates on predicting the hover performance of an isolated rotor with emphasis on accurate representation of the shed wake. The CFD method of Ramachandran, et. al. [1] is a technique that has demonstrated the ability to preserve the shed rotor wake. The key to this approach, called Vorticity Embedding, is the use of velocity decomposition coupled with Lagrangian wake convection. This is a transonic, potential-based method having the unique ability to convect free circulation without numerical dissipation. This freedom from numerical dissipation permits the use of fairly sparse grids (a typical grid contains 250,000 points, which includes blade surface resolution). Such grids together with the inherent speed of having to only solve for mass conservation result in a numerical method that is uniquely practical. This method is implemented in the code HELIX-I [1].

The stand-alone version of HELIX-I utilizes a single-block H-grid topology which is very good for accurately resolving the rotor wake since the grid lines are almost always parallel to the shed wake. However, an H-grid topology is not very good for resolving blade loads since the leading-edge grid is singular. Furthermore, stand-alone HELIX-I utilizes a simple integral boundary-layer model to estimate the total power. This works very well for cases in which the flow is not strongly three-dimensional and does not approach stall. However, for general problems where separation is possible, the use of Navier-Stokes methods, which mostly rely upon C-grid topologies, is required.

In an effort to predict improved blade loads, Moulton et al. [2] developed a hybrid Navier-Stokes/Vorticity Embedding model to analyze hover. To avoid errors related to interpolation, the method combined a C-grid version of the well-known HELIX-I code with the TURNS Navier-Stokes code [3] to provide the near-blade flow solution. Although the method was fast and grid point efficient, it was determined that significant errors in wake convection were produced in the region of the C-grid upstream of and below the blade where the grid lines transition from being parallel to the wake to being perpendicular to the wake. Prescribed-wake solutions compared very well with published data and demonstrated the viability of the hybrid methodology.

The next logical step in the development was to combine the two topologies using an overset method. That is, the inviscid flow field, modeled by Vorticity Embedding, was treated with a two-grid overset version of the HELIX-I code. The outer H-grid was governed only by wake accuracy considerations, while an inner C-type grid was governed by the need to model the surface inviscid flow or make the transition to a near-blade viscous solver. This overset/hybrid approach was outlined by Moulton et al. [4].

Previous applications of the overset/hybrid method were limited to prescribed-wake simulations and hybridized the inner C-grid to transition to a near-blade viscous solution. This paper describes the current state of development of the free-wake capability of the overset/hybrid solver and exercises the option to extend the inner C-grid to the blade surface. For the first time, the lowest level of fidelity for the overset/hybrid method (a two-grid overset potential-based flow) will be demonstrated for isolated rotor hover simulations.

2. METHODOLOGY

In general, the overset/hybrid method utilizes three grid topologies (see Fig. 1): a background H-grid to accurately convect the shed rotor wake; an intermediate C-grid to allow the coupling of a near-blade viscous solver with the inviscid solver along coincident grid lines; and a near-blade C-grid to resolve the viscous flow including separation effects. The following discussion gives a description of the flow solvers for each region along with appropriate boundary conditions to exchange flow information. Boundary condition requirements for the two-grid overset option of the method is emphasized.

2.1 Inviscid Region

The inviscid region includes the outer H-grid for wake convection as well as the intermediate C-grid which either permits a smooth coupling with the near-blade viscous region or extends to the blade surface. This flow is

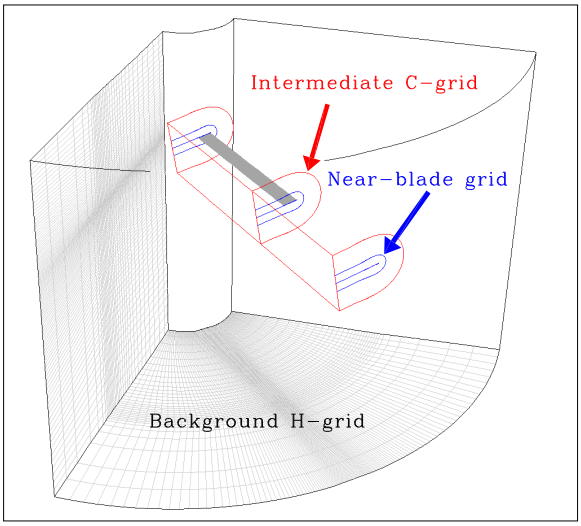

Fig. 1. Features of an overset/hybrid grid for a rotor in hover.

governed by the steady, full–potential equation written in generalized coordinates [5],

$$\frac{\partial}{\partial\xi}\left(\frac{\rho U}{J}\right)+\frac{\partial}{\partial\eta}\left(\frac{\rho V}{J}\right)+\frac{\partial}{\partial\zeta}\left(\frac{\rho W}{J}\right)=0 \qquad (1)$$

where (U,V,W) are the contravariant velocities and J is the Jacobian of the transformation evaluated using

$$J=\frac{1}{det(\mathcal{H})} \qquad (2)$$

with

$$\mathcal{H}=\begin{pmatrix} x_\xi & x_\eta & x_\zeta \\ y_\xi & y_\eta & y_\zeta \\ z_\xi & z_\eta & z_\zeta \end{pmatrix}. \qquad (3)$$

The physical velocity components,

$$\vec{q}=\begin{pmatrix} u \\ v \\ w \end{pmatrix}=\left(\mathcal{H}^T\right)^{-1}\begin{pmatrix} \Phi_\xi \\ \Phi_\eta \\ \Phi_\zeta \end{pmatrix}+\vec{\Omega}\times\vec{r}+\vec{q}_v, \qquad (4)$$

are required to compute the contravariant velocities. Note that Φ is the velocity potential; $\vec{\Omega}\times\vec{r}$ accounts for the rotating coordinate frame ($\vec{r}$ denotes the radial location); $\vec{q}_v$ corresponds to the vortical velocity which is a result of the Vorticity Embedding technique which is explained below. The density, ρ, is determined from the steady, compressible Bernoulli equation,

$$\rho=\left\{1+\frac{\gamma-1}{2}\left[M_T^2(\vec{\Omega}\times\vec{r})^2-\vec{q}\cdot\vec{q}\right]\right\}^{\frac{1}{\gamma-1}} \qquad (5)$$

where M_T is the tip Mach number. The above equations (Eqns. 1 and 5) are nondimensionalized the same as Eqn. 8.

The full-potential equation is solved using a semi-implicit, finite-volume scheme [6] and results in a computer code called HELIX-I. The most attractive feature of HELIX-I is the inclusion of Vorticity Embedding.

The basis of the Vorticity Embedding method is to decompose the velocity into potential and rotational components,

$$\vec{q}=\nabla\Phi+\vec{q}_v \qquad (6)$$

where $\vec{q}_v$ represent the rotational or vortical component of the total velocity. This decomposition introduces a forcing term into the standard full-potential equation. In general, the vortical velocity field is not known and is constructed by assuming the following form

$$\vec{q}_v=\Gamma\nabla\lambda \qquad (7)$$

where Γ (circulation) and λ are Clebsch variables and represent the local strength and geometry of the shed wake, respectively.

The following steps outline the basic solution procedure for the flow about a hovering rotor (also see the flowchart in Fig. 2).

step 1: The first step in the analysis is to locate the wake. For steady flows, the shed circulation is constant along streamlines that emanate from the trailing edge of the rotating blade. Therefore, particles or wake markers are injected along the radius of the blade and convected downstream to the outflow boundary. The convection time step is chosen such that each Eulerian grid cell contains at least one Lagrangian wake node. In general, the wake node locations do not coincide with the Eulerian grid points. Therefore, the local velocity at the node is determined by trilinear interpolation of the velocities at the surrounding grid points.

Upon reaching the downstream boundary, the wake elements are transferred to the periodic upstream boundary and serve as an initial condition for the integration of the next sheet segment. This process is repeated as necessary to complete the description of the wake geometry. For this analysis, four sheet segments are freely convected and represent the near wake region. The far wake is defined as the region between the last computed sheet segment and the bottom boundary. In this region, the wake is extrapolated from the last computed sheet.

step 2: After determining the geometry of the shed rotor wake, the vortex sheet is spread in computational space. That is, the circulation of the convecting Lagrangian wake nodes are impressed on the adjacent grid points as a local vortical velocity distribution. This procedure is completely described in Ref. [7].

step 3: The velocity potential is updated using the mass balance relation along with the Bernoulli equation.

step 4: Repeat steps 1-3 until the Lagrangian wake nodes do not change position.

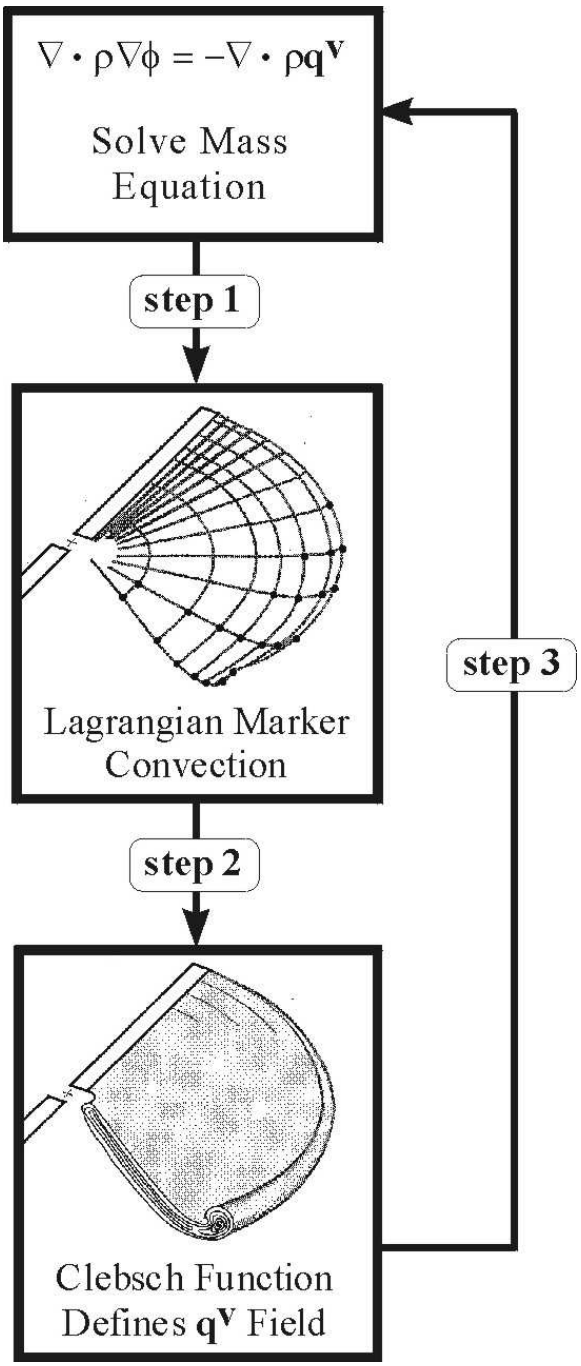

Fig. 2. Iterative process used for the Vorticity Embedding procedure

Since the original development of this method, improvements have been made to the free-wake procedure which has resulted in a new version of the code called HELIX-IA; see Refs. [8] and [9] for an overview of the enhancements. In spite of extensive improvements, it is still extremely difficult to generate a surface-conforming grid that resolves both the local blade flow and the wake flow. The primary difficulty seems to arise from the blade leading edge region where the H-topology is singular. Since the H-grid is ideal for wake convection, it was desirable to retain this topology. Therefore, two modes of operation for HELIX-IA were developed to alleviate the problems associated with surface-conforming H-grids. These two modes are described as follows

"lifting surface" mode: The "lifting-surface" mode for HELIX-IA represents the blade by a flat lifting-surface along the blade chord. The magnitude of the sectional lift is obtained from the bound circulation using the Kutta-Joukowski theorem. The effective inflow angle (or tilt of the lift vector) is estimated by using the Weissinger-L model (see Ref. [8] for its implementation into HELIX-IA). It is noteworthy that the use of a lifting-surface grid is not inherent to the method. Rather, good results obtained with this simple grid make it difficult to justify a more detailed grid.

"lifting-line" mode: When a higher level of fidelity is desired for the blade surface solution (e.g. a near-blade viscous solution), a surface-conforming grid is unnecessary for convection of the shed rotor wake. In fact, the lifting-surface can be reduced to a lifting-line at the leading edge of the blade. For this mode, the blade bound circulation must be specified from external information. This mode of operation is ideally suited for the overset/hybrid computation process where the bound circulation is derived from an inner blade solution.

2.2 Viscous Region

For cases where the near-blade C-grid is utilized, the blade flow is computed using the unsteady, thin-layer Navier-Stokes equations written in generalized coordinates [3],

$$\frac{\partial \hat{Q}}{\partial \tau} + \frac{\partial \hat{E}}{\partial \xi} + \frac{\partial \hat{F}}{\partial \eta} + \frac{\partial \hat{G}}{\partial \zeta} = Re^{-1} \frac{\partial \hat{S}}{\partial \zeta} + \hat{\mathcal{R}} \qquad (8)$$

where Re is the Reynold's number. The solution vector $(\hat{Q})$ is given by

$$\hat{Q} = J^{-1} \begin{pmatrix} \rho \\ \rho u \\ \rho v \\ \rho w \\ e \end{pmatrix}. \qquad (9)$$

$(\hat{E}, \hat{F}, \hat{G})$ are the inviscid flux vectors. The viscous flux vector, $\hat{S}$, utilizes the thin-layer approximation. Since a noninertial coordinate system is employed, the addition of a source term, $\hat{\mathcal{R}}$, is required to account for the centrifugal acceleration of the rotating blades [10].

An implicit, finite-difference scheme is used to solve Eqn. 8. The resulting computer code is called TURNS (Transonic Unsteady Rotor Navier-Stokes) [11]. Salient features of TURNS are listed below. The inviscid fluxes are computed using an upwind-biased flux-difference scheme with flux limiters to model shocks. Using Roe's

upwinding eliminates the need for explicit numerical dissipation. The flux limiters lead to a TVD (total variation diminishing) scheme which improves the spatial accuracy to second- or third-order. The implicit operator is solved using a Lower-Upper-Symmetric Gauss-Seidel scheme.

2.3 Boundary Conditions

Recall that HELIX-IA provides two modes of operation: "lifting-surface" mode for stand-alone operation and "lifting-line" mode for wake-only operation (i.e. blade loads are supplied by an auxiliary means). The wake-only operation provides a simple means to interface with an inner C-grid topology. The procedure employed by Moulton et al. [4] accomodated hole points in the outer H-grid topology. The new procedure obviates this requirement since the blade loads are impressed along a lifting-line in the outer H-grid. This freedom also simplifies the grid generation process.

The following describes the boundary conditions required to advance the solution from the outer H-grid topology to the inner, intermediate C-grid topology.

1. The potential on the outer boundary of the intermediate C-grid is obtained from the H-grid. Additionally, the intermediate C-grid requires the vortical velocity field (which represents the shed rotor wake) from the outer H-grid. Since these two grids are not coincident, the velocity potential must be determined by searching and interpolating the solution from the H-grid. This search and interpolation is performed by utilizing routines that are a subset of the well-known code called PLOT3D [12].

2. The inner grid topology consists of a single block C-H grid topology that is constructed by stacking two-dimensional C-grids in the radial direction. Off the tip of the blade, the grid is collapsed to form a double-line resulting in a beveled tip. The near-blade loading can be determined in two ways

   (a) The intermediate C-grid can be extended to the blade surface thereby producing inviscid loads. The boundary condition enforces zero normal flow at the surface. This option also requires that the wake shed from the trailing edge reside on the doubly-defined cut on the C-grid. Along this cut, the standard velocity potential jump is applied.

   (b) The C-grid can be decomposed into viscous and inviscid regions by specifying the outer location of the near-blade region and the number of overlap cells. At the interface boundary of the near-blade region, a Dirichlet condition is provided by the full–potential solution. That is, the vector of conserved variables, Eqn. 9, is constructed using the velocity field from the inviscid region. The interface boundary condition supplied to the potential flow solver is the mass flux and density constructed from the near-blade solution (see Ref. [13] for details pertaining to interface boundary conditions).

3. The near-blade loading is then passed to the outer H-grid wake solver (HELIX-IA) as bound circulation.

4. This iterative process of cycling between the outer wake solver and inner blade solution is continued until convergence.

3. VALIDATION STUDIES

For this study, a 4-bladed Knight and Hefner (K-H) rotor [14] is examined to evaluate the free-wake capability of the overset/hybrid procedure. However, since the data only contains integrated performance polars, the computed overset results are also compared to predictions using the hybrid option of the code [15]. Furthermore, it is appropriate to compare two-grid overset results to stand-alone HELIX-IA results since both simulate potential flow for the entire domain.

To identify the levels of fidelity of the overset/hybrid results, the two-grid overset approach described herein will be referred to as HELIXC and the option to hybridize the intermediate C-grid with an inner TURNS solution is referred to as HELIXC/TURNS [15]. Prescribed-wake results are shown first to demonstrate the overset capability of the methodology. These predictions are followed by free-wake simulations to demonstrate the utility of the new two-grid overset option.

3.1 Prescribed-Wake Simulations

This first simulation is intended to demonstrate the utility of the new two-grid overset option. By prescribing the outer flow from a stand-alone HELIX-IA solution and reducing the thickness of the K-H blade to zero (a flat-plate), any discrepancies between the two results can be isolated to boundary condition implementation.

Consider the inviscid flow ($M_T = 0.23, Re_c = \infty$) about a hovering K-H rotor ($\theta_{.75} = 10^\circ, AR = 15.0, t/c = 0.0$). Figure 3 shows a composite of the overset grids. The dotted lines represent the H-H grid topology, which has 126 points in the azimuthal direction (26 points near the blade surface), 107 points in the axial direction (62 points below the plane of the blade) and 33 radial planes (25 on the blade). The far field boundaries are approximately located one-half rotor radius above and one rotor radius below the rotor disk. The inboard and outboard radial boundaries are located at 0.25R and 1.6R, respectively.

Figure 4 shows the overset topologies near the rotor blade at $r/R = 0.75$. The intermediate C-grid used in the potential calculation has 193 points in the wrap-around direction (145 points on the surface), 48 points in the normal direction with a spacing of $0.005c$ at the surface and 33 radial planes (26 on the blade). The outer boundary is

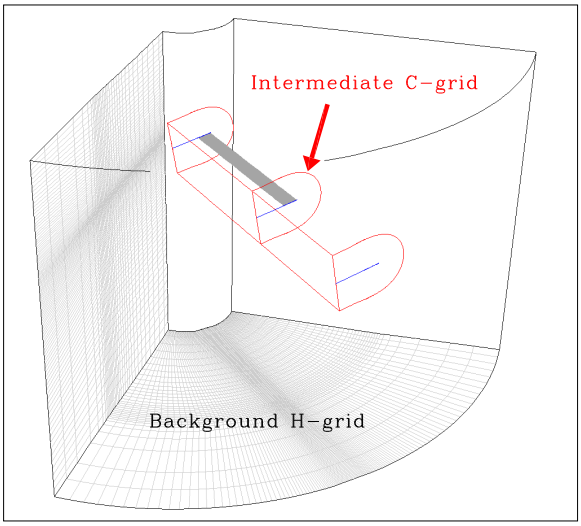

Fig. 3. Features of an overset/hybrid grid for the K-H rotor in hover ($\theta_{.75} = 10^\circ, AR = 15.0$).

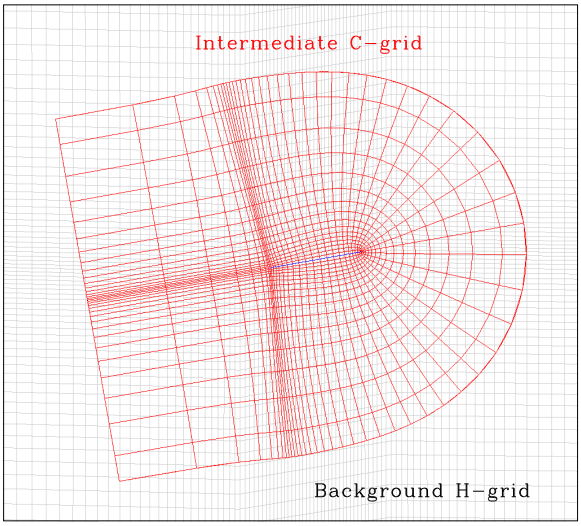

Fig. 4. Overset grids at $r/R = 0.75$ for the K-H rotor ($t/c = 0.0$) in hover ($\theta_{.75} = 10^\circ, AR = 15.0$).

located approximately $2.0c$ from the rotor blade (as measured from the leading edge).

Figure 5 shows a comparison of the predicted surface pressure coefficients with that resulting from stand-alone HELIX-IA. The comparison is very good even though the near wake (that portion of the shed wake that resides within the C-grid) model is different. Clearly, both blade solutions see the same shed rotor wake.

Figure 6 illustrates the salient features of the current methodology by depicting the wake as constant vorticity iso-surfaces (only a small radial portion near the blade tip is shown for clarity). The tip marker trajectory from stand-alone HELIX-IA is also shown. Vorticity on the boundary of the intermediate C-grid clearly shows the tip vortex entering the hybrid region. Also evident in the figure is the tip vortex formation captured in the near-blade region. The overall induced inflow, as well as the vortex passage effects, are injected into the inner solution through the interface conditions along the intermediate grid outer boundary. Therefore, the resulting blade solution includes the effect of the wake induced inflow as modeled by the outer HELIX-IA solution.

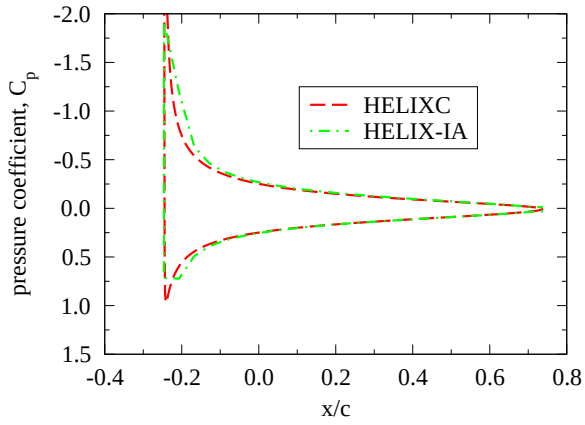

Fig. 5. Surface pressure coefficient distribution at $r/R = 0.65$ for the K-H rotor blade ($t/c = 0.0$) in hover ($\theta_{.75} = 10^\circ, M_T = 0.23, Re_c = \infty$).

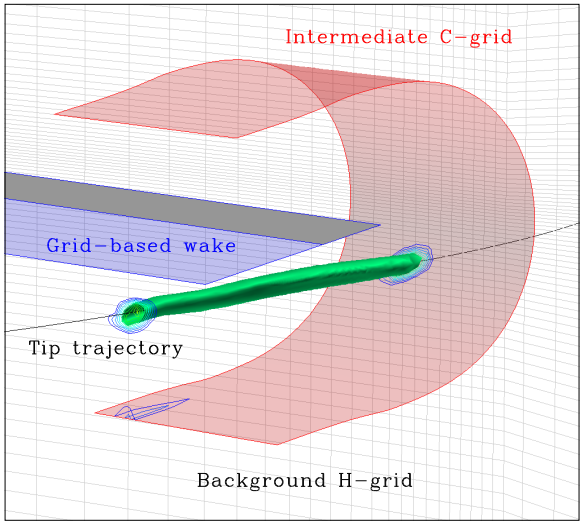

Fig. 6. Illustration of tip vortex formation in the intermediate C-grid region that was interpolated from the background HELIX-IA solution ($\theta_{.75} = 10^\circ, M_T = 0.23, Re_c = \infty$).

3.2 Free-Wake Simulations

The previous results clearly show that the two-grid overset methodology is consist with stand-alone HELIX-IA results. Next, free-wake simulations are performed to further validate the overset procedure. Overset topologies near the rotor blade for the these calculations are nearly identical to those used in the previous section. However, the free-wake solutions correctly model the NACA0015 thickness effects (see Fig. 7).

For a collective pitch setting of 10 degrees, the computed wake geometry is shown in Fig. 8. Only the free-wake shed from one blade is shown to emphasize the ge-

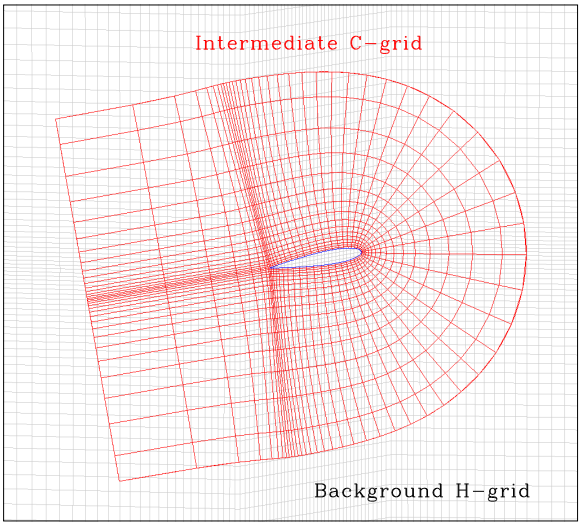

Fig. 7. Overset grids at $r/R = 0.75$ for the K-H rotor in hover ($\theta_{.75} = 10^\circ, AR = 15.0$).

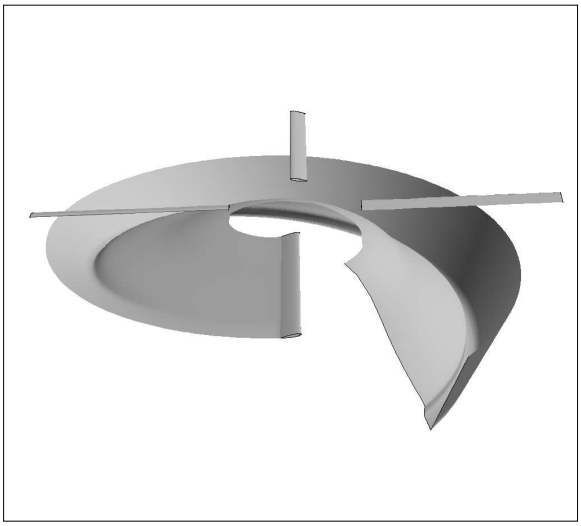

Fig. 8. Lagrangian representation of the computed shed wake for the K-H rotor in hover ($\theta_{.75} = 10^\circ, M_T = 0.23, Re_c = \infty$).

ometry of the Lagrangian sheet of markers. The far wake (the portion of wake beyond the wake nodes shown in the figure) is azimuthally extrapolated from the last 90 degrees of computed markers, which is equivalent to assuming a rigid, non-contracting wake.

The predicted HELIXC tip vortex trajectory compares fairly well with the stand-alone HELIX-IA predictions, see Fig. 9. However, the stand-alone HELIX-IA wake is axially closer to the blade which indicates that the rotor is operating at a lower thrust which is confirmed in Fig. 10 where the variation of thrust with collective pitch setting is shown. Clearly, the overset results are overpredicting the test data and stand-alone HELIX-IA results. However, if you take into account thickness effects, the results are encouraging.

Next, viscous simulations are performed to further

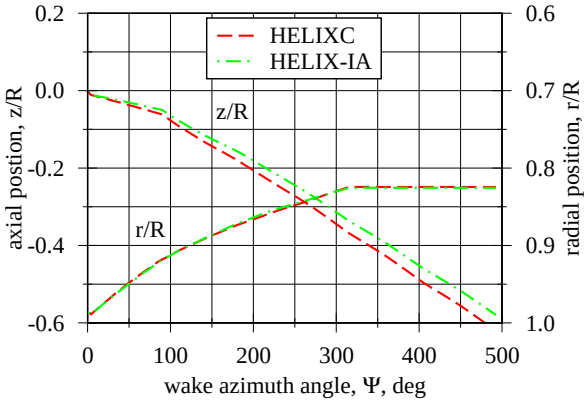

Fig. 9. Comparison of computed tip vortex trajectory with HELIX/TURNS and stand-alone HELIX-IA ($\theta_{.75} = 10^\circ, M_T = 0.23, Re_c = \infty$).

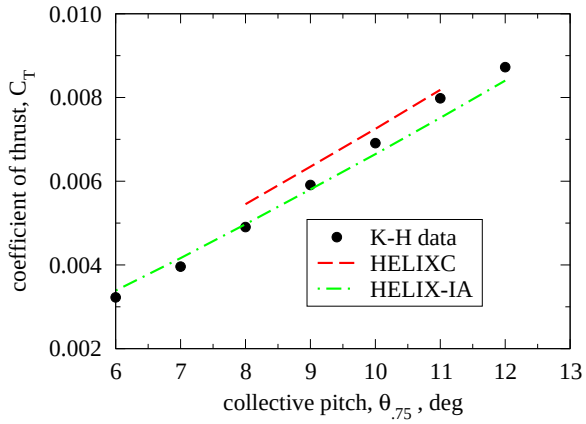

Fig. 10. Comparison of computed thrust coefficient with K-H data ($M_T = 0.23, Re_c = \infty$).

substantiate the thickness effect and validate the free-wake procedure. To exercise this option of the overset/hybrid method, the near-blade grid is simply extracted from the intermediate C-grid by choosing the outer boundary location of the near-blade grid, approximately $0.5c$ (see Fig. 11). The viscous grid is completed by enriching the first 5 normal grid cells with 50 cells resulting in 77 points in the normal direction with a spacing of $0.00002c$ at the surface.

The sweep of collective pitch settings used previously was repeated for the viscous simulations ($M_T = 0.23, Re_c = 242,000$). Clearly, the two overset/hybrid results are overpredicting the test data and stand-alone HELIX-IA results, see Fig. 12. Nevertheless, it is encouraging that the overset/hybrid results are consistent with each other. For $\theta_{.75} = 10^\circ$ (shown in Fig. 13), the predicted overset/hybrid trajectories also compare very well with each other, but differ from the stand-alone HELIX-IA result. In summary, the new two-grid overset option for the overset/hybrid method is consistent with hybrid results. Difference between overset/hybrid results and HELIX-IA results is attributed to thickness effects.

With confidence in the two-grid overset results, it

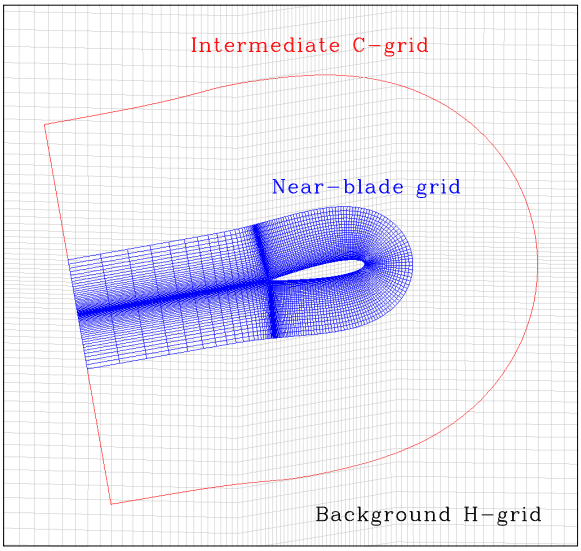

Fig. 11. Overset/hybrid grids at r/R = 0.75 for the K-H rotor in hover ($\theta_{.75} = 10°, AR = 15.0$).

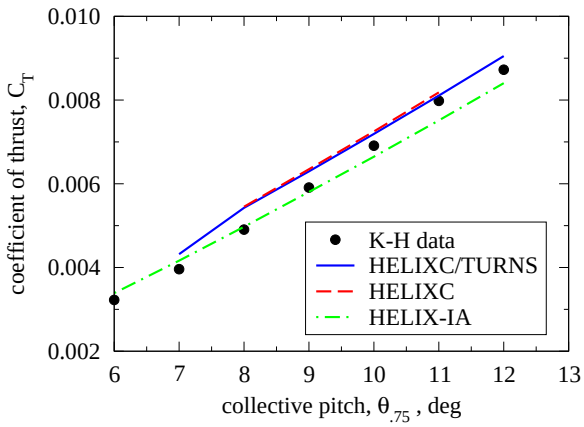

Fig. 12. Comparison of computed thrust coefficient with K-H data and HELIXC/TURNS ($M_T = 0.23, Re_c = 242,000$).

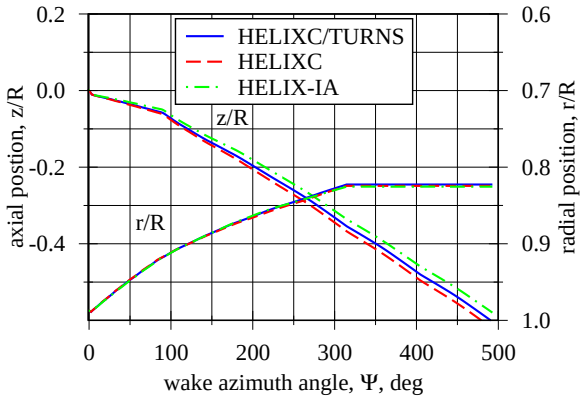

Fig. 13. Comparison of computed tip vortex trajectory (axial and radial) with HELIXC/TURNS and stand-alone HELIX-IA ($\theta_{.75} = 10°, M_T = 0.23, Re_c = 242,000$).

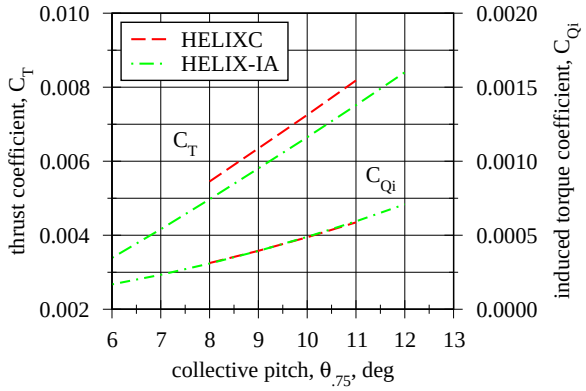

Fig. 14. Comparison of computed integrated performance coefficients with stand-alone HELIX-IA ($M_T = 0.23, Re_c = \infty$).

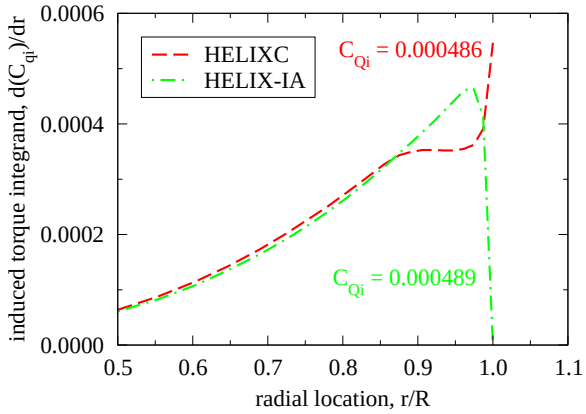

Fig. 15. Comparison of predicted spanwise sectional torque coefficient with stand-alone HELIX-IA ($M_T = 0.23, Re_c = \infty$).

is possible to assess the Weissinger-L model used in HELIX-IA to estimate the induced torque. As seen in Fig. 14, it is surprising that the induced torque shows no dependency upon thickness. Furthermore, for $\theta_{.75} = 10°$, the distributions of the sectional torque, see Fig. 15, between the two methods are different, particularly near the blade tip. At this point, these differences are not understood and represent an area of further investigation.

4. SUMMARY & CONCLUSIONS

This paper presents free-wake hover results obtained using an overset/hybrid CFD method that combines an outer Vorticity Embedded potential solver with a near-blade viscous solver. The inviscid flow field is treated with a two-grid overset version of the HELIX-I code. The outer H-grid is governed only by wake accuracy considerations, while the inner C-grid is either governed by the need to make the transition to a near-blade Navier-Stokes solver or extend to the surface to resolve inviscid blade loads. The two-grid overset procedure was simplified by utilizing the "wake-only" option of HELIX-IA (an enhanced version of HELIX-I). The goal of this work is

to provide a general viscous/free-wake CFD solver with sufficient accuracy and efficiency for engineering application.

An evaluation of the two-grid overset option of the overset/hybrid code was presented for a 4-bladed, hovering K-H rotor. Predictions were compared against available test data. The inviscid predictions were also compared to stand-alone HELIX-IA results. However, since the test data was limited to integrated performance quantities, the predictions were also compared against the overset/hybrid code utilizing the viscous near-blade grid.

First, prescribed-wake simulations were compared to stand-alone HELIX-IA results to demonstrate the accuracy of the two-grid overset method. Recall that the stand-alone HELIX-IA code utilizes a lifting-surface to compute blade loads. Therefore, to produce a result free of thickness effects, the overset results were performed using a zero-thickness flat plate. For a 10 degree collective pitch setting, the overset results compared very well with the stand-alone HELIX-IA results. The slight discrepancies in the surface pressure coefficients are attributed to differences in the surface grid resolutions (the C-grid is much finer near the leading edge). Nevertheless, the comparison clearly shows that the blade loads reflect the same induced flow which implies that the influence of the shed wake is properly modeled in the context of the new overset methodology.

With the free-wake option enabled, the overset method was run at several collective pitch settings to generate performance data for the K-H rotor blade. The predicted thrust overpredicted both the experimental and HELIX-IA data. The difference between the two computed results is due to thickness effects. Comparison of tip vortex trajectories with stand-alone HELIX-IA confirmed the difference in loading. To further evaluate the overset method, the predicted results were also compared to overset/hybrid results where a near-blade viscous grid was employed. The thrust comparison was very good which was confirmed by a good comparison with tip vortex trajectories.

Recall that stand-alone HELIX-IA relies upon the Weissinger-L model to estimate induced torque. With confidence in the new two-grid overset option, the predicted results were examined to assess this model. Although the overset results overpredicted the HELIX-IA thrust, the induced torque between the two were virtually the same. To further confuse the issue, the radial distribution of torque was very different at the tip. At this point, these differences are not understood and require further study.

The present work is under active development and the following recommendations should be considered. First and foremost, a study should be conducted to further assess the Weissinger-L model. Although not covered in the paper, the intermediate C-grid solver is based upon the original HELIX-I technology. It is desirable to update this to the current HELIX-IA technology. Finally, the new overset option of the overset/hybrid code should be used to predict loading distributions and performance for the UH-60A model blade. Here the blade characteristics are more complex and should give a qualitative measure of the capabilities of this approach.

Inclusion of the previously mentioned studies/capabilities will further advance the overset/hybrid methodology into a general engineering analysis tool. The fidelity of the flow model ranges from purely potential (the new two-grid overset option) to a hybrid method to resolve viscous effects near the blade surface. It would especially valuable for the study of high lift configurations, such as tilt rotors.

ACKNOWLEDGMENTS

The present paper represents over twenty years of development, beginning with an ARO (Army Research Office) sponsored Ph.D. thesis at the University of Tennessee Space Institute (UTSI). In the subsequent years, development has been supported by the Army Aeroflightdynamics Directorate (AFDD) at Ames Research Center, California. Other support for this work has come from the U.S. Army Aviation and Missile Research, Development & Engineering Center in Huntsville, Alabama.

REFERENCES

[1]Ramachandran, K., Tung, C., and Caradonna, F., "Rotor Hover Performance Using a Free Wake, CFD Method," *Journal of Aircraft*, Vol. 26, (12), Dec 1989, pp. 1105–1110.

[2]Moulton, M. A., Ramachandran, K., Hafez, M. M., and Caradonna, F. X., "Hover Performance Prediction Using CFD," American Helicopter Society Specialist Meeting on Aeromechanics Technology and Product Design for the 21st Century, Bridgeport, CT, October 11–13, 1995.

[3]Srinivasan, G. R., Baeder, J., Obayashi, S., and McCroskey, W. J., "Flowfield of a Lifting Rotor in Hover," *AIAA Journal*, Vol. 30, (10), October 1992, pp. 2371–2378.

[4]Moulton, M. A., Bridgeman, J. O., and Caradonna, F. X., "Development of an Overset/Hybrid CFD Method for the Prediction of Hover Performance," American Helicopter Society 53^{rd} Annual Forum Proceedings, Virginia Beach, VA, April 29–May 1, 1997.

[5]Steinhoff, J. S. and Ramachandran, K., "Free Wake Analysis of Helicopter Rotor Blades in Hover Using a Finite Volume Technique," Report DAAG29-84-K-0019, U. S. Army Research Office, Research Triangle Park, NC, October 1988.

[6]Steinhoff, J. S. and Suryanarayana, K., "The Treatment of Vortex Sheets in Compressible Potential Flow," Proceedings of the AIAA Symposium on Computational Fluid Dynamics, Danvers, July 1983.

[7]Moulton, M., "Zonal Procedure for Predicting the Hover Performance of a Helicopter Rotor," PhD thesis, University of California-Davis, Sept. 1998.

[8]Bhagwat, M. J., Moulton, M. A., and Caradonna, F. X., "Development of a CFD-based Hover Performance Prediction Tool for Engineering Analysis," AHS 61*st* Annual National Forum, Grapevine, TX, June 2005.

[9]Bhagwat, M. J., Harris, F. D., Moulton, M. A., and Caradonna, F. X., "Development and Application of a CFD-based Engineering Analysis of Hover Performance," AHS 62*nd* Annual National Forum, Phoenix, AZ, May 2006.

[10]Vinokur, M., "An Analysis of Finite-Difference and Finite-Volume Formulations of Conservation Laws," *Journal of Computational Physics*, Vol. 81, (1), Mar. 1989, pp. 1–52.

[11]Srinivasan, G., "A Free-Wake Euler and Navier-Stokes CFD Method and its Application to Helicopter Rotors Including Dynamic Stall," JAI Associates Technical Report, Nov. 1993.

[12]Walatka, T. L., Buning, T. G., Pierce, L., and Elson, P. A., "PLOT3D User's Manual," NASA TM 101067, March 1990.

[13]Moulton, M. A., Wenren, Y., and Caradonna, F. X., "Free-Wake Hover Flow Prediction with a Hybrid Potential/Navier-Stokes Solver," Proceedings of the 55th Annual Forum of the American Helicopter Society International, Montréal Cananda, May 25–27 1999.

[14]Knight, M. and Hefner, R. A., "Static Thrust Analysis of The Lifting Airscrew," Technical Report TN 626, NACA, December 1937.

[15]Moulton, M. A., Bhagwat, M. J., and Caradonna, F. X., "Hybrid CFD Methods for the Prediction of Isolated Rotor Hover Performance," International Forum on Rotorcraft Multidisciplinary Technology Proceedings, Seoul, Korea, October 15–17, 2007.